Monthly Notices
of the
ROYAL ASTRONOMICAL SOCIETY

MNRAS **492,** 3553–3565 (2020)
Advance Access publication 2020 January 10

doi:10.1093/mnras/staa003

Signatures of bimodality in nebular phase Type Ia supernova spectra

P. J. Vallely [1]★ M. A. Tucker,[2] B. J. Shappee,[2] J. S. Brown,[1,3] K. Z. Stanek[1,4] and C. S. Kochanek[1,4]

[1]*Department of Astronomy, The Ohio State University, 140 West 18th Avenue, Columbus, OH 43210, USA*
[2]*Institute for Astronomy, University of Hawai'i, 2680 Woodlawn Drive, Honolulu, HI 96822, USA*
[3]*Department of Astronomy and Astrophysics, University of California, Santa Cruz, CA 95064, USA*
[4]*Center for Cosmology and AstroParticle Physics, The Ohio State University, 191 W. Woodruff Ave., Columbus, OH 43210, USA*

Accepted 2019 December 27. Received 2019 December 6; in original form 2019 January 31

ABSTRACT

One observational prediction for Type Ia supernovae (SNe Ia) explosions produced through white dwarf–white dwarf collisions is the presence of bimodal velocity distributions for the ^{56}Ni decay products, although this signature can also be produced by an off-centre ignition in a delayed detonation explosion. These bimodal velocity distributions can manifest as double-peaked or flat-topped spectral features in late-time spectroscopic observations for favourable viewing angles. We present nebular-phase spectroscopic observations of 17 SNe Ia obtained with the Large Binocular Telescope. Combining these observations with an extensive search of publicly available archival data, we collect a total sample of 48 SNe Ia and classify them based on whether they show compelling evidence for bimodal velocity profiles in three features associated with ^{56}Ni decay products: the [Fe II] and [Fe III] feature at ∼5300 Å, the [Co III] λ5891 feature, and the [Co III] and [Fe II] feature at ∼6600 Å. We identify nine bimodal SNe in our sample, and we find that these SNe have average peak M_V about 0.3 mag fainter than those that do not. This is consistent with theoretical predictions for explosions created by nearly head-on collisions of white dwarfs due to viewing angle effects and ^{56}Ni yields.

Key words: techniques: spectroscopic – supernovae: general.

1 INTRODUCTION

Type Ia supernovae (SNe Ia) are important objects in astronomy. With luminosities of $\sim 10^{43}$ erg s^{-1} at maximum light, they can be detected and monitored out to considerable distances. SNe Ia are best known for their use as cosmological standardizable candles, arising from the tight correlation discovered by Phillips (1993) between their peak M_B and their rate of decline $\Delta m_{15}(B)$. Riess et al. (1998) and Perlmutter et al. (1999) took advantage of this relationship to discover the accelerating expansion of the Universe. Beyond cosmology, SNe Ia also play an important role in our understanding of nucleosynthesis, as they are one of the primary sources of iron-group and intermediate-mass elements, have a significant impact on the gas dynamics and star formation characteristics of galaxies, and are likely sources of high-energy cosmic rays (see e.g. Maoz, Mannucci & Nelemans 2014).

Despite the importance of SNe Ia, our knowledge of the events themselves is still far from complete. The most pressing questions surround the nature of their progenitors and explosion mechanism. SN Ia explosions are the thermonuclear detonations of carbon–oxygen white dwarfs (CO WDs; Hoyle & Fowler 1960; Colgate & McKee 1969), and a companion is required to trigger the explosion. The details of the explosion mechanism are unknown and remain an active topic of discussion. Possible progenitor scenarios can be broadly divided into two channels: one involving a companion star still undergoing thermonuclear burning (the single-degenerate or SD scenario), and one involving a WD companion (the double-degenerate or DD scenario).

In the canonical SD scenario, a CO WD accretes hydrogen-rich or helium-rich material from a non-degenerate companion until it approaches the Chandrasekhar limit, at which point it experiences a thermonuclear runaway and explodes (Whelan & Iben 1973; Han & Podsiadlowski 2004). There has also been considerable work done to study possible sub-Chandrasekhar (Woosley & Weaver 1994; Sim et al. 2010; Shen & Moore 2014) and super-Chandrasekhar (Yoon, Langer & Scheithauer 2004; Yoon & Langer 2005; Hachisu, Kato & Nomoto 2012) SD channel explosions. In the standard DD scenario, a tight WD binary loses energy and angular momentum to gravitational wave emission before undergoing tidal interactions and subsequently exploding as a SN Ia (Iben & Tutukov 1984; Webbink 1984; Shen et al. 2012). The complete theoretical landscape for SNe Ia is considerably more complex, including numerous proposed explosion mechanisms for both scenarios. Popular mechanisms include the delayed detonation (Khokhlov 1991; Woosley & Weaver 1994; Livne 1999) and double detonation (Woosley, Weaver & Taam

★ E-mail: vallely.7@osu.edu

1980; Nomoto 1982; Bildsten et al. 2007; Shen & Moore 2014) models. More exotic mechanisms like the violent prompt merger scenario, an SD variant where a WD merges with the degenerate core of an asymptotic giant branch star, have also been considered (Livio & Riess 2003; Soker et al. 2013).

All of these progenitor channels have varying degrees of theoretical and observational problems. For instance, most SD scenario channels require finely tuned accretion rates in order for the WD to successfully gain mass and explode (Starrfield et al. 1972; Nomoto 1982; Iben & Tutukov 1984). Additionally, observational evidence for such progenitor systems has proven to be elusive. The nearby SNe Ia 2011fe and 2014J were particularly well studied (Brown et al. 2012; Munari et al. 2013; Foley et al. 2014; Goobar et al. 2014; Mazzali et al. 2014; Galbany et al. 2016; Vallely et al. 2016; Shappee et al. 2017; Yang et al. 2018), but no compelling evidence was found for the existence of non-degenerate companions (Bloom et al. 2012; Chomiuk et al. 2012; Shappee et al. 2013; Margutti et al. 2014; Lundqvist et al. 2015).

Extensive searches for hydrogen emission lines at late times as evidence for stripped companion material have largely failed (Mattila et al. 2005; Leonard 2007; Lundqvist et al. 2013; Maguire et al. 2016; Graham et al. 2017; Sand et al. 2018; Holmbo et al. 2019; Sand et al. 2019; Tucker, Shappee & Wisniewski 2019). Indeed, in an unparalleled sample of over 100 SNe Ia, Tucker et al. (2019) found no evidence for the predicted emission signatures. To date, only two normal Type Ia SNe, ASASSN-18tb (Brimacombe et al. 2018) and ATLAS18qtd (Prieto et al. 2019), show compelling evidence for strong Hα emission (Kollmeier et al. 2019). However, Vallely et al. (2019) showed that the hydrogen signature in ASASSN-18tb is likely a product of CSM interaction and not indicative of an SD progenitor system. In contrast, Prieto et al. (2019) find that the Hα emission observed in ATLAS18qtd is broadly consistent with the signatures expected for stripped companion material, although they note that the inferred hydrogen mass of $\sim 10^{-3}$ M$_{\odot}$ is significantly below classical SD theoretical model predictions.

Fine-tuning is also generally required for DD scenario mergers to avoid off-centre ignitions and accretion-induced collapse to a neutron star (Nomoto & Iben 1985; Shen et al. 2012; Moll et al. 2014). Extensive discussion of SNe Ia progenitor systems and explosion mechanisms and their respective theoretical and observational challenges can be found in Hillebrandt et al. (2013), Maoz et al. (2014), Branch & Wheeler (2017), and Ashall et al. (2018).

Another possible progenitor scenario is the collisional WD channel. In this variant of the DD scenario, rather than slowly inspiralling due to gravitational wave emission, the two WDs collide nearly head-on – virtually guaranteeing explosion due to the strong shocks produced in the collision (Hawley, Athanassiadou & Timmes 2012; García-Senz et al. 2013; Kushnir et al. 2013). This scenario was first raised as a potential explanation for a small fraction of observed SNe Ia in dense stellar regions (Rosswog et al. 2009b; Raskin et al. 2009, 2010). The Kozai–Lidov effect (Kozai 1962; Lidov 1962) in triple systems may make this channel relatively generic (Thompson 2011; Antognini et al. 2014). Katz & Dong (2012) argue that the rate of direct WD collisions may nearly equal that of observed SNe Ia, although the extent of this collision rate enhancement is debated by Hamers et al. (2013) and Toonen, Perets & Hamers (2018).

The collisional WD channel provides fairly straightforward observable predictions. In particular, the velocity distribution of the ^{56}Ni deposited in the ejecta of these explosions is intrinsically bimodal (Dong et al. 2015). At appropriate viewing angles, these bimodal velocity distributions will manifest as double-peaked or flat-topped spectral features in late-time spectroscopic observations of ^{56}Ni decay products. Upon examining archival nebular phase spectra of SNe Ia, Dong et al. (2015) confidently identified signatures of bimodality in 3 of the 18 SNe in their sample, indicating that SNe Ia exhibiting this predicted characteristic are not uncommon.

This is not a unique observable of the collisional WD channel, however, as bimodal ^{56}Ni distributions can also be produced by an off-centre delayed detonation (Fesen et al. 2007; Gerardy et al. 2007). In this explosion mechanism, the supernova explosion begins as a subsonic deflagration wave at the centre of the WD and propagates outwards. The deflagration transitions into a supersonic detonation front when the density at its leading edge crosses a critical transition density (Khokhlov 1991; Woosley & Weaver 1994; Livne 1999). This transition is not perfectly understood, so the value of this critical density is chosen such that the model replicates observed characteristics of SNe Ia (Höflich, Khokhlov & Wheeler 1995; Höflich et al. 2003). A significant quantity of off-centre ^{56}Ni is produced during the detonation phase (Höflich et al. 2002; Gerardy et al. 2007). Off-centre delayed detonations are generally considered in the context of SD progenitor systems, but they can also occur in the DD case (Piersanti et al. 2003). The degeneracy between WD collisions and off-centre delayed-detonations can be broken using detailed radiative transfer calculations to analyse the observations (Mazzali et al. 2018).

In this paper, we present nebular-phase spectroscopic observations of 17 nearby SNe Ia obtained over the past few years using the Large Binocular Telescope (LBT; Hill, Green & Slagle 2006). Most of these spectra were obtained as part of a long-term effort to accumulate a complete volume-limited spectroscopic sample of SNe Ia nebular phase observations out to $z \sim 0.2$. Once complete, the nebular spectra for 100 SNe Ia (Dong et al. 2018) survey will be an invaluable resource for our understanding of SNe Ia and their progenitors. Among the sample we present here, we identify two events that are consistent with an underlying bimodal velocity distribution. We then combine these spectra with a sample of 31 additional archival nebular phase SNe Ia observations presented in Tucker et al. (2019), where we identify an additional seven events showing evidence of bimodality. We show that these bimodal SNe Ia are systematically less luminous at peak than their single velocity component counterparts, and we discuss how this may arise from viewing angle dependent effects inherent to the collisional WD scenario or ^{56}Ni production.

This paper is organized as follows. In Section 2.1, we describe the LBT observations we undertook to obtain 18 spectra of 17 nearby SNe Ia during the nebular phase. In Section 2.2, we describe the sources from which we obtained our archival sample of nebular phase spectra and near-peak photometry, and we also provide a brief description of the methods we used to convert the observed *V*-band observations into absolute magnitudes. In Section 3, we describe the classification methods we use to determine whether or not spectra show evidence of a bimodal velocity distribution. Finally, in Section 4 we demonstrate that bimodal SNe Ia are less luminous than SNe Ia in general, and we discuss our findings in the context of the SNe Ia progenitor problem.

2 THE SAMPLE

2.1 Previously unpublished observations

All of the new spectra we present here were obtained using the MULTIOBJECT DOUBLE SPECTROGRAPHs mounted on the twin 8.4m

LBT (MODS1 and MODS2; Pogge et al. 2010). The MODS1 spectra were reduced using a combination of the MODSCCDRED[1] PYTHON package, and the MODSIDL pipeline.[2] Unfortunately, some of the calibration data necessary to use the MODSIDL pipeline are not yet available for MODS2, so the MODS2 observations were reduced using standard techniques in IRAF to extract and calibrate the 1D spectra in wavelength and flux. Spectra of SNe 2016ehy, 2016ffh, 2016fnr, and ASASSN-16lx were obtained using only MODS2 data because MODS1 was not operational during those observations. All other spectra were obtained using only MODS1 data. Due to the relatively high sky noise in the red channel, the spectrum of 2016bry could only be extracted in the blue channel and is excluded from futher analysis.

The properties of these spectroscopic observations are summarized in Table 1, and Fig. 1 shows the 18 LBT spectra we obtained for this paper. Broadly speaking, the spectroscopic properties of our sample are comparable to the sample presented by Graham et al. (2017). All of the spectra show prominent emission features in various ^{56}Ni decay products, and the [Fe III] λ4701 emission feature is particularly strong in all of the spectra. In our analysis, we focus on three neighbouring Fe/Co emission features: the [Fe II] and [Fe III] blended feature at ∼5300 Å, the [Co III] λ5891 feature, and the [Fe II] and [Co III] blended feature at ∼6600 Å.

An in-depth discussion justifying the use of these features can be found in appendix B of Dong et al. (2015). In short, they are chosen because they are narrow, well characterized, and nearly identical between the spectra of SNe 1991bg and SN 1999by. The structure of the [Fe III] λ4701 feature, on the other hand, differs significantly between the two SNe and appears to be strongly impacted by complicated blends of nearby lines, rendering it unsuitable for our analysis. We are limited to these optical features only due to the wavelength ranges of the spectra in our sample. In principle, an underlying bimodal velocity distribution of ^{56}Ni should manifest in all late-time Fe/Co features, and as we discuss in Section 3, this allows us to verify our identifications using the results of studies at non-optical wavelengths.

We restrict our analysis to spectra with S/N > 10 and coverage of at least two of the pertinent Fe/Co features. This leads to the exclusion of the spectra for SNe 2016bry, 2016ehy, and 2016eqa. As we discuss further in Section 3, the spectra of SNe 2014bv and 2016iuh are particularly interesting, as they show fairly compelling evidence of bimodal velocity distributions in their ^{56}Ni ejecta.

2.2 Archival data

We also utilize a subset of the exhaustive sample of spectroscopic archival late-time SNe Ia observations we collected and present in Tucker et al. (2019). To obtain this sample, we systematically extracted spectra from a number of archival data bases, including the Weizmann Interactive Supernova Data Repository (Yaron & Gal-Yam 2012), the Open Supernova Catalog (Guillochon et al. 2017), the Berkeley SuperNova Ia Program (Silverman et al. 2009, 2012), the Carnegie Supernova Project (CSP; Folatelli et al. 2013), and the Center for Astrophysics Supernova Program (Blondin et al. 2012). We also present a number of previously unpublished spectra reduced from raw data available in other public archives. See Tucker et al. (2019) for a detailed description of how we obtained the full sample. The spectroscopic properties of the SNe we utilize in our analysis are summarized in Table 2.

We restrict our sample to events with reasonably well-sampled near-peak *V*-band light curves, so that we can compare the peak luminosities of the bimodal events with the overall sample. The photometric properties of these archival SNe Ia are summarized in Table 3. Only *Swift* UVOT observations were obtained for a few of these events, and in these instances we use UVOT *V*-band observations in lieu of Johnson *V*-band observations. We identify these events in Table 3. In cases where both were obtained, we use the Johnson *V* observations.

With the exception of the extreme cases of SNe 1986G, 2002er, and 2014J, we do not correct for host galaxy extinction. It seems unlikely that there would be any preference for bimodal events to occur along high or low extinction lines of sight, so for our relative comparison of peak M_V this should be of no major concern. We account for Galactic foreground extinction using the Schlafly & Finkbeiner (2011) infrared-based dust map, and we use redshift-independent estimates of the distance modulus (μ) for SNe with $z < 0.01$.

3 DETERMINING BIMODALITY

In the majority of cases, detecting signatures of bimodality in the ^{56}Ni velocity profiles of a spectrum can be performed fairly reliably by inspection. For instance, one can visually identify double-peaked Fe/Co features in the late-time spectra of SN 2007on and SN 2014bv, indicating possible bimodal velocity profiles. Similarly, a cursory examination of the late-time spectra of SN 2011fe and SN 2012cg shows no need to invoke anything beyond standard single-component velocity broadening. However, there are also events such as SNe 2016iuh and 2012ei that do not fall cleanly into either category. In order to handle the classification of these borderline events self-consistently, and to minimize the impact of any potential bias, it is best to have an objective classification scheme.

We use the direct convolution technique described by Dong et al. (2015), although our implementation differs slightly. We construct a bimodal velocity kernel using two quadratic components, and then convolve this kernel with a template SN Ia nebular phase spectrum. Due to its narrow emission features and particularly high S/N, we retain from Dong et al. (2015) the use of SN 1999by for this pre-convolution template. This phase + 180d SN 1999by template spectrum is shown by the blue line in Fig. 2.

The velocity convolution kernel is described by

$$\frac{\mathrm{d}M}{\mathrm{d}v_{\mathrm{LOS}}} \propto P_1 + r \cdot P_2, \text{ where} \tag{1}$$

$$P_1 = \max\left(1 - \frac{(v_{\mathrm{LOS}} - v_{\mathrm{shift},1})^2}{\sigma^2_{\mathrm{mod},1}}, 0\right), \tag{2}$$

$$v_{\mathrm{shift},1} = v_{\mathrm{shift}} - \frac{1}{2}v_{\mathrm{sep}}, \tag{3}$$

$$P_2 = \max\left(1 - \frac{(v_{\mathrm{LOS}} - v_{\mathrm{shift},2})^2}{\sigma^2_{\mathrm{mod},2}}, 0\right), \text{ and} \tag{4}$$

$$v_{\mathrm{shift},2} = v_{\mathrm{shift}} + \frac{1}{2}v_{\mathrm{sep}}. \tag{5}$$

There are five free parameters: the shifts of the two components $v_{\mathrm{shift},1}$ and $v_{\mathrm{shift},2}$, the widths of the two components $\sigma_{\mathrm{mod},1}$ and $\sigma_{\mathrm{mod},2}$, and the peak ratio of the components r. The shifts are described using the two parameters of velocity shift, $v_{\mathrm{shift}} = \frac{1}{2}(\sigma_{\mathrm{mod},1} + \sigma_{\mathrm{mod},2})$, and velocity separation, $v_{\mathrm{sep}} = v_{\mathrm{shift},2} - v_{\mathrm{shift},1}$.

[1] http://www.astronomy.ohio-state.edu/MODS/Software/modsCCDRed/
[2] http://www.astronomy.ohio-state.edu/MODS/Software/modsIDL/

Table 1. LBT spectroscopic observations.

SN	Obs. date	Phase (d)	z	Exposure (s)	Wavelength coverage	Bimodal Fe/Co
SN 2012ei	2013-05-03	230	0.006 57	4800	3470–8940 Å	No
SN 2014bv	2015-04-22	292	0.005 59	10 800	3480–9440 Å	**Yes**
SN 2014J	2014-11-21	292	0.000 68	12 600	3490–9490 Å	No
SN 2014J	2015-01-21	353	0.000 68	10 800	3490–9490 Å	No
SN 2015I	2016-02-08	269	0.007 59	10 800	3470–9420 Å	No
ASASSN-15uh	2016-06-14	165	0.013 50	3600	3450–9370 Å	No
SN 2016bry[b]	2016-11-20	198	0.016 02	2700	3440–5600 Å	Noisy
SN 2016coj	2016-11-18	162	0.004 48	2700	3480–9450 Å	No
SN 2016ehy[a]	2017-03-02	231	0.045 00	3600	3340–8130 Å	Noisy
SN 2016eqa	2016-11-20	105	0.014 96	5400	3440–9360 Å	Noisy
SN 2016ffh[a]	2017-03-02	181	0.018 20	3600	3430–8340 Å	No
SN 2016fnr[a]	2017-03-02	164	0.014 37	3600	3450–8370 Å	No
SN 2016gxp	2017-05-27	213	0.017 85	3600	3430–9330 Å	No
ASASSN-16lx[a]	2017-03-02	134	0.018 60	3600	3430–8340 Å	No
SN 2016iuh	2017-05-27	164	0.013 70	7200	3450–9370 Å	**Yes [Co III]**
ASASSN-17cz	2017-05-28	87	0.017 38	2700	3440–9330 Å	No
SN 2017hjw	2018-03-14	135	0.016 16	2700	3440–9340 Å	No
ASASSN-17pg	2018-03-14	106	0.005 62	1800	3480–9440 Å	No

Notes. The wavelength coverage is reported for the rest frame of each spectrum.
[a]MODS2 spectra.
[b]The red channel spectrum had too low an S/N to effectively extract from the observations.

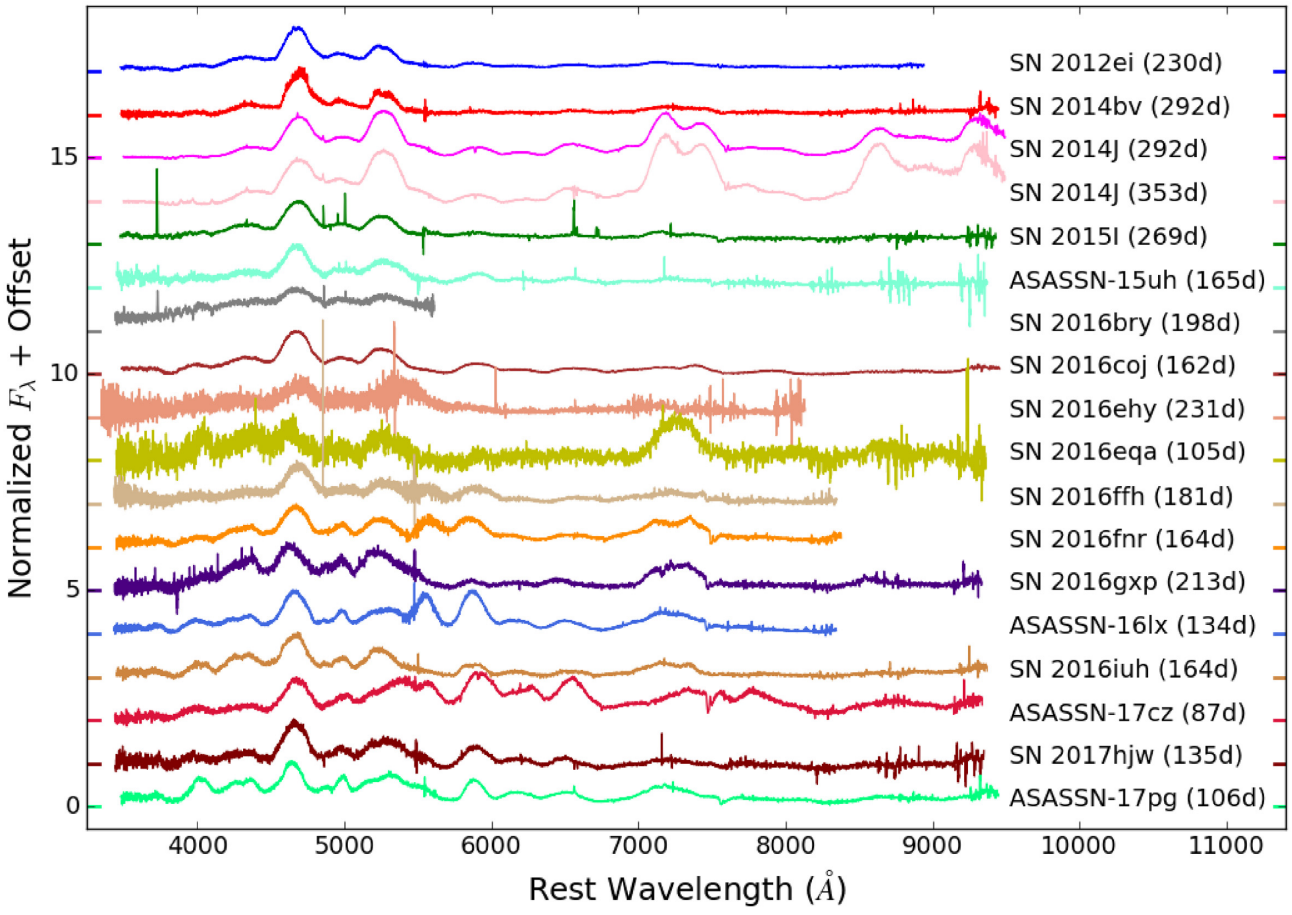

Figure 1. The new LBT late-time SNe Ia spectra we present in this paper. Phases relative to maximum V-band brightness are indicated in parentheses next to each spectrum. The coloured tick marks on the vertical axes indicate the offset used when plotting each spectrum, and all spectra are normalized to the peak of the [Fe III] λ4701 emission feature. This feature is prominent in all of the spectra, as are numerous other signatures of ^{56}Ni decay products. We restrict our analysis to spectra with S/N $>$ 10 and coverage of at least two of the pertinent Fe/Co features. These spectra are available in machine-readable format in the online version of the paper.

Table 2. Spectroscopic properties.

SN	z	Type	Phase (d)	Bimodal Fe/Co	Reference(s)
SN 2012cg	0.00146	Ia-Norm	284	No	Shappee et al. (2018)
SN 2014bv	0.00559	Ia-Norm	292	**Yes**	This work
SN 2014J	0.00068	Ia-Norm	292,353	No	This work
SN 2015I	0.00759	Ia-Norm	269	No	This work
SN 2016coj	0.00448	Ia-Norm	162	No	This work
SN 2016fnr	0.01437	Ia-Norm	164	No	This work
SN 2016gxp	0.01785	Ia-91T	213	No	This work
SN 2016iuh	0.01370	Ia-91bg	164	**Yes [Co III]**	This work
SN 2017hjw	0.01616	Ia-Norm	135	No	This work
ASASSN-15uh	0.01350	Ia-91T	165	No	This work
ASASSN-16lx	0.01860	Ia-Norm	134	No	This work
ASASSN-17cz	0.01738	Ia-Norm	87	No	This work
ASASSN-17pg	0.00562	Ia-Norm	106	No	This work
ASASSN-14jg	0.01483	Ia-Norm	216	No	Tucker et al. (2019)
SN 1981B	0.00603	Ia-Norm	113,267	No	Branch et al. (1983), Richardson et al. (2001)
SN 1986G	0.00180	Ia-91bg	256	**Yes**	Ruiz-Lapuente & Lucy (1992)
SN 1989B	0.00243	Ia-Norm	150	No	Wells et al. (1994)
SN 1990N	0.00340	Ia-Norm	184,225,253,278	No	Gómez & López (1998)
SN 1991T	0.00579	Ia-91T	183[1], 255[2], 281[2], 313[2], 317[1]	No	[1]Silverman et al. (2012); [2]Gómez & López (1998)
SN 1998aq	0.00370	Ia-Norm	230,240	No	Blondin et al. (2012)
SN 1998bu	0.00299	Ia-Norm	190[1], 208[1], 217[1], 236[2], 243[1], 280[2], 329[3]	No	[1]Blondin et al. (2012); [2]Silverman et al. (2012); [3]Cappellaro et al. (2001)
SN 1999aa	0.01444	Ia-91T	256	No	Silverman et al. (2012)
SN 1999by	0.00213	Ia-91bg	181	No	Silverman et al. (2012)
SN 2000cx	0.00793	Ia-Pec	181	No	Blondin et al. (2012)
SN 2002dj	0.00939	Ia-Norm	218,271	No	Pignata et al. (2008)
SN 2002er	0.00857	Ia-Norm	214	**Yes [Co III]**	Kotak et al. (2005)
SN 2003du	0.00638	Ia-Norm	219	No	Stanishev et al. (2007)
SN 2003gs	0.00477	Ia-Pec	197	**Yes**	Silverman et al. (2012)
SN 2003hv	0.00560	Ia-Norm	319	**Yes**	Leloudas et al. (2009)
SN 2004bv	0.01061	Ia-Norm	159	No	Silverman et al. (2012)
SN 2004eo	0.01570	Ia-Norm	226	No	Pastorello et al. (2007a)
SN 2005am	0.00790	Ia-Norm	297,380	**Yes**	Leonard (2007)
SN 2005cf	0.00646	Ia-Norm	264	No	Leonard (2007)
SN 2007af	0.00546	Ia-Norm	301	No	Blondin et al. (2012)
SN 2007le	0.00672	Ia-Norm	304	No	Silverman et al. (2012)
SN 2007on	0.00649	Ia-Norm	284	**Yes**	Folatelli et al. (2013)
SN 2008A	0.01646	Ia-02cx	201,225	No	McCully et al. (2014)
SN 2008Q	0.00794	Ia-Norm	201	No	Silverman et al. (2012)
SN 2011by	0.00284	Ia-Norm	204,308	No	Silverman, Ganeshalingam & Filippenko (2013)
SN 2011fe	0.00080	Ia-Norm	205[1], 226[1], 229[2], 259[1], 347[1]	No	[1]Mazzali et al. (2015); [2]Shappee et al. (2013)
SN 2011iv	0.00649	Ia-Norm	244,261	**Yes**	Gall et al. (2018)
SN 2012fr	0.00540	Ia-Norm	220,259,338,365	No	Childress et al. (2015)
SN 2012hr	0.00756	Ia-Norm	281	No	Childress et al. (2015)
SN 2013aa	0.00400	Ia-Norm	188,205,345	No	Childress et al. (2015)
SN 2013dy	0.00389	Ia-Norm	332	No	Pan et al. (2015)
SN 2013gy	0.01402	Ia-Norm	271	No	Childress et al. (2015)
SN 2015F	0.00489	Ia-Norm	194,293	No	Tucker et al. (2019)
SN 2017cbv	0.00400	Ia-Norm	315	No	Tucker et al. (2019)

Note. That phases are calculated in the observed frame relative to maximum *V*-band brightness.

We limit our analysis to three features we can confidently associate with ^{56}Ni decay products: the [Fe II] and [Fe III] feature at ∼5300 Å, the [Co III] λ5891 feature, and the [Co III] and [Fe II] feature at ∼6600 Å. The [Co III] λ5891 feature is particularly valuable due to its lack of multiline blending. We obtain fits for each spectrum by varying the velocity kernel parameters ($v_{\rm shift}$, $\sigma_{\rm mod,\,1}$, $\sigma_{\rm mod,\,2}$, $v_{\rm sep}$, and r) to minimize χ^2 for two cases – one fit using only the [Co III] λ5891 feature, and one fit using all three of the pertinent ^{56}Ni decay features. The fit parameters of the spectra we show in Figs 2–5 are provided in Table 4. In all figures, the convolution fit to the ∼5300 Å [Fe II]/[Fe III] feature is shown in red, the convolution fit to the [Co III] λ5891 feature is shown in orange, and the convolution fit to the ∼6600 Å [Co III]/[Fe II] feature is shown in green.

We classify the spectral fits as being consistent with a bimodal velocity profile if the two quadratic components of the velocity kernel do not significantly overlap – that is, $v_{\rm sep} \gtrsim \sigma_{\rm mod,1} + \sigma_{\rm mod,2}$. Two spectra representative of the single-component events which do not satisfy this criteria are shown in Fig. 3. While there are benefits to using only the [Co III] feature – namely that it is not subject to blending concerns – we regard identifications made using all three features as more robust. These identifications are shown in Fig.

Table 3. Peak *V*-band brightness.

SN	m_V	Dist. mod. (μ)	Extinction (A_V)	M_V	Reference(s)
SN 2012cg	11.90[1]	31.02[2]	0.057	– 19.18	[1]Vinkó et al. (2018); [2]Munari et al. (2013)
SN 2014bv[a]	13.92[1]	32.17[2]	0.106	– 18.36	[1]Brown et al. (2014); [2]Tully et al. (2013)
SN 2014J	10.56[1]	27.64[2]	0.435 + 1.76[b]	– 19.28	[1]Tsvetkov et al. (2014); [2]Dalcanton et al. (2009); [2]Marion et al. (2015)
SN 2015I[a]	13.99[1]	32.64[2]	0.182	– 18.83	[1]Brown et al. (2014); [2]Tully et al. (2013)
SN 2016coj	13.02[1]	31.90[2]	0.052	– 18.93	[1]Kochanek et al. (2017); [2]Blakeslee et al. (2001)
SN 2016fnr	15.28[1]	33.98	0.128	– 18.83	[1]Kochanek et al. (2017)
SN 2016gxp	14.84[1]	34.55	0.338	– 20.05	[1]Chen & Dong (in preparation)
SN 2016iuh	15.43[1]	33.88	0.045	– 18.49	[1]Kochanek et al. (2017)
SN 2017hjw	15.85[1]	34.24	0.370	– 18.76	[1]Chen & Dong (in preparation)
ASASSN-15uh	15.28[1]	33.85	0.410	– 18.98	[1]Kochanek et al. (2017)
ASASSN-16lx	15.47[1]	34.55	0.115	– 19.20	[1]Kochanek et al. (2017)
ASASSN-17cz	16.60[1]	34.33	1.138	– 18.86	[1]Chen & Dong (in preparation)
ASASSN-17pg	14.46[1]	32.51[2]	0.145	– 18.19	[1]Kochanek et al. (2017); [2]Tully, Courtois & Sorce (2016)
ASASSN-14jg	14.92[1]	34.05	0.042	– 19.17	[1]Kochanek et al. (2017)
SN 1981B	11.85[1]	30.83[2]	0.050	– 19.03	[1]Barbon, Ciatti & Rosino (1982); [2]Tully et al. (2013)
SN 1986G	11.44[1]	27.82[2]	1.95[c]	– 18.33	[1]Phillips et al. (1987); [2]Tully et al. (2013)
SN 1989B	11.99[1]	29.78[2]	0.091	– 17.88	[1]Wells et al. (1994); [2]Tully et al. (2013)
SN 1990N	12.73[1]	31.72[2]	0.071	– 19.06	[1]Lira et al. (1998); [2]Tully et al. (2013)
SN 1991T	11.51[1]	30.91[2]	0.060	– 20.00	[1]Lira et al. (1998); [2]Parodi et al. (2000)
SN 1998aq	12.46[1]	31.67[2]	0.039	– 19.25	[1]Riess et al. (2005); [2]Tully et al. (2013)
SN 1998bu	11.86[1]	30.11[2]	0.069	– 18.32	[1]Jha et al. (1999); [2]Tully et al. (2013)
SN 1999aa	14.90[1]	34.10[1]	0.109	– 19.31	[1]Kowalski et al. (2008)
SN 1999by	13.14[1]	30.82[2]	0.054	– 17.73	[1]Garnavich et al. (2004); [2]Tully et al. (2013)
SN 2000cx	13.23[1]	32.40[2]	0.224	– 19.39	[1]Li et al. (2001); [2]Takanashi, Doi & Yasuda (2008)
SN 2002dj	14.13[1]	32.65[2]	0.261	– 18.78	[1]Hicken et al. (2009); [2]Tully et al. (2013)
SN 2002er	14.59[1]	32.51[2]	1.12[d]	– 19.04	[1]Pignata et al. (2004); [2]Tully et al. (2013)
SN 2003du	13.57[1]	32.83[2]	0.027	– 19.29	[1]Hicken et al. (2009); [2]Tully et al. (2013)
SN 2003gs	13.49[1]	31.49[2]	0.097	– 18.10	[1]Krisciunas et al. (2009); [2]Blakeslee et al. (2001)
SN 2003hv	12.55[1]	31.55[2]	0.042	– 19.04	[1]Leloudas et al. (2009); [2]Tully et al. (2013)
SN 2004bv	14.02[1]	32.80[2]	0.174	– 18.95	[1]Ganeshalingam et al. (2010); [2]Tully et al. (2013)
SN 2004eo	15.33[1]	34.12[1]	0.296	– 19.09	[1]Pastorello et al. (2007a)
SN 2005am	13.76[1]	32.24[2]	0.147	– 18.63	[1]Ganeshalingam et al. (2010); [2]Tully et al. (2013)
SN 2005cf	13.50[1]	32.32[2]	0.267	– 19.09	[1]Pastorello et al. (2007b)
SN 2007af	13.21[1]	31.76[2]	0.107	– 18.66	[1]Hicken et al. (2009); [2]Tully et al. (2013)
SN 2007le	13.66[1]	31.73[2]	0.092	– 18.16	[1]Hicken et al. (2012); [2]Springob et al. (2009)
SN 2007on	12.96[1]	31.45[2]	0.032	– 18.52	[1]Contreras et al. (2010); [2]Tully et al. (2013)
SN 2008A	16.09[1]	34.05	0.149	– 18.11	[1]Ganeshalingam et al. (2010)
SN 2008Q	13.75[1]	32.30	0.227	– 18.78	[1]Ganeshalingam et al. (2010)
SN 2011by[a]	12.92[1]	32.01[2]	0.038	– 19.13	[1]Brown et al. (2014); [2]Maguire et al. (2012)
SN 2011fe	9.97[1]	29.05[2]	0.024	– 19.10	[1]Munari et al. (2013); [2]Vinkó et al. (2012)
SN 2011iv	12.38[1]	31.45[2]	0.031	– 19.10	[1]Gall et al. (2018); [2]Tully et al. (2013)
SN 2012fr	11.98[1]	31.25[2]	0.056	– 19.33	[1]Contreras et al. (2018); [2]Tully et al. (2013)
SN 2012hr[a]	13.75[1]	33.03[2]	0.124	– 19.40	[1]Brown et al. (2014); [2]Tully et al. (2013)
SN 2013aa[a]	11.62[1]	30.55[2]	0.466	– 19.40	[1]Brown et al. (2014); [2]Bottinelli et al. (1985)
SN 2013dy	12.94[1]	30.68[2]	0.421	– 18.16	[1]Zhai et al. (2016); [2]Tully et al. (2009)
SN 2013gy	14.77[1]	33.75	0.158	– 19.14	[1]Graham et al. (2017)
SN 2015F	13.27[1]	31.64[2]	0.556	– 18.93	[1]Graham et al. (2017); [2]Cartier et al. (2017)
SN 2017cbv	11.64[1]	30.13[2]	0.463	– 18.95	[1]Chen & Dong (in preparation); [2]Bottinelli et al. (1985)

Notes. The foreground Galactic extinction A_V values are taken from Schlafly & Finkbeiner (2011).
[a]Johnson *V* observations were not obtained, so *Swift* UVOT *V* observations are substituted.
[b]SN 2014J exhibits considerable host galaxy extinction, so we adopt the $A_V = 1.76$ host galaxy extinction value from Tsvetkov et al. (2014).
[c]SN 1986G exhibits considerable host galaxy extinction, so we adopt $E(B - V) = 0.63$ from di Serego-Alighieri & Ponz (1987) and assume $R_V = 3.1$ to obtain $A_V = 1.95$.
[d]SN 2002er exhibits considerable host galaxy extinction, so we adopt $E(B - V) = 0.36$ from Pignata et al. (2004) and assume $R_V = 3.1$ to obtain $A_V = 1.12$.

4. It is very unlikely that a single-component velocity distribution can produce similarly spaced double-peaked profiles for the three well-separated features. For robust identification using the triple-feature fit, we strictly require $v_{\rm sep} > \sigma_{\rm mod,1} + \sigma_{\rm mod,2}$, while for the more tentative [Co III] feature identifications we allow for a small overlap of 500 km s^{-1} provided that the two kernel components are still largely distinct from one another and satisfy $\sigma_{\rm mod,1} < v_{\rm sep}$ and $\sigma_{\rm mod,2} < v_{\rm sep}$ (see Fig. 5).

In nearly all cases where the three-feature fit produces a bimodal classification, the single [Co III] feature fit does so as well. Of the six events classified as bimodal using the multifeature fit, only in the case of SN 2003hv does the single [Co III] feature fit disagree. Upon

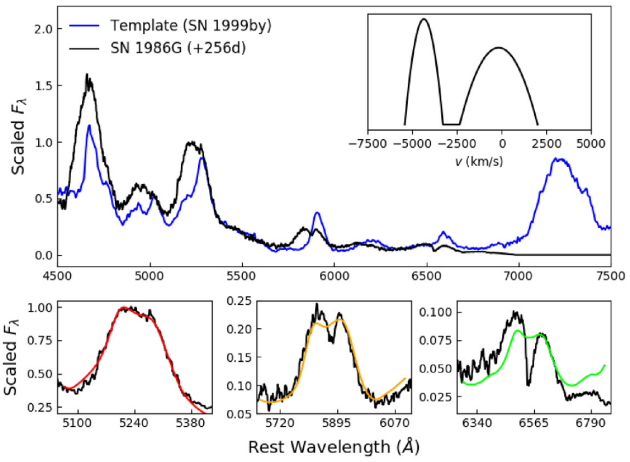

Figure 2. An illustration of our convolution-based fitting technique. The nebular phase spectrum of SN 1986G is shown in black, and the SN 1999by spectrum we adopt as a pre-convolution template throughout the paper is shown in blue. The template spectrum is convolved with the velocity kernel plotted in the upper right-hand panel to produce the feature-specific fits in the lower panels. As in all figures, the convolution fit to the ∼5300 Å [Fe II]/[Fe III] feature is shown in red, the convolution fit to the [Co III] λ5891 feature is shown in orange, and the convolution fit to the ∼6600 Å [Co III]/[Fe II] feature is shown in green. Complications in the interpretation of the SN 1986G spectrum are discussed in Section 3.

inspection of the SN 2003hv spectrum, one notes that the [Co III] λ5891 feature, although not double peaked, shows a flat-top profile consistent with a bimodal velocity profile. Our sample includes 14 of the 18 SNe considered by Dong et al. (2015). We recover the bimodal classifications found by Dong et al. (2015) for SNe 2007on, 2003gs, and 2005am. Using our triple-feature fit criteria, we classify SNe 2008Q and 2003hv, which Dong et al. (2015) had described as ambiguous identifications, as single-component and bimodal events, respectively.

It is encouraging to note that the results of our classification scheme generally agree with the results of nebular phase spectral modeling studies. Mazzali et al. (2018) find that fitting the nebular phase spectra of SN 2007on and SN 2011iv requires two-component models, consistent with the bimodal identification we obtain for each event. No secondary component is required when modelling SN 2011fe (Mazzali et al. 2015), SN 1991T (Sasdelli et al. 2014), or SN 2004eo (Mazzali et al. 2008), as expected for events we classify as single component.

Near-infrared (NIR) observations are also consistent with our classification scheme. We identify SN 2003hv as a bimodal event, and flat-topped profiles of the [Fe II] 1.257 and 1.644 μm features indicate that it is indeed an asymmetric explosion (Motohara et al. 2006). Meanwhile, there are no such indications in NIR observations of SN 2014J, which we classify as a single-component event (Dhawan et al. 2018).

In addition to the six bimodal events, we confidently identify through multifeature fitting, we identify two events where the [Co III] λ5891 feature is consistent with bimodality even though the best multifeature fit does not satisfy our classification criterion. The spectra of these two events – SNe 2016iuh and 2002er – are shown in Fig. 5. Although we regard these identifications as less robust than those obtained through the multifeature fits, they are nevertheless meaningful and we find no obvious problems when we examine the spectra manually. Particularly in the case of SN 2002er, the structure of the [Co III] feature is clearly double peaked. The [Co III] feature could be affected by Na I D absorption. However, its colour excess of $E(B-V) = 0.36$ corresponds to an Na I D equivalent width of ∼1.2 Å (Pignata et al. 2004; Poznanski, Prochaska & Bloom 2012) that is nearly three times smaller than the absorption feature observed in the spectrum. While Phillips et al. (2013) showed that there is significant dispersion in this relation, it is unlikely that the double peaks in this feature can be explained as a product of host extinction. Furthermore, we find that the peak absolute magnitude of these two events are very similar to those identified through multifeature fitting.

SN 1986G presents a unique challenge and warrants further discussion. Our best-fitting convolution model to this spectrum is shown in Fig. 2 and is clearly consistent with a bimodal identification under the classification scheme described above. However, this event suffers from considerable host galaxy extinction, and the presence of absorption from the Na I D doublet (λλ5890, 5896) com-

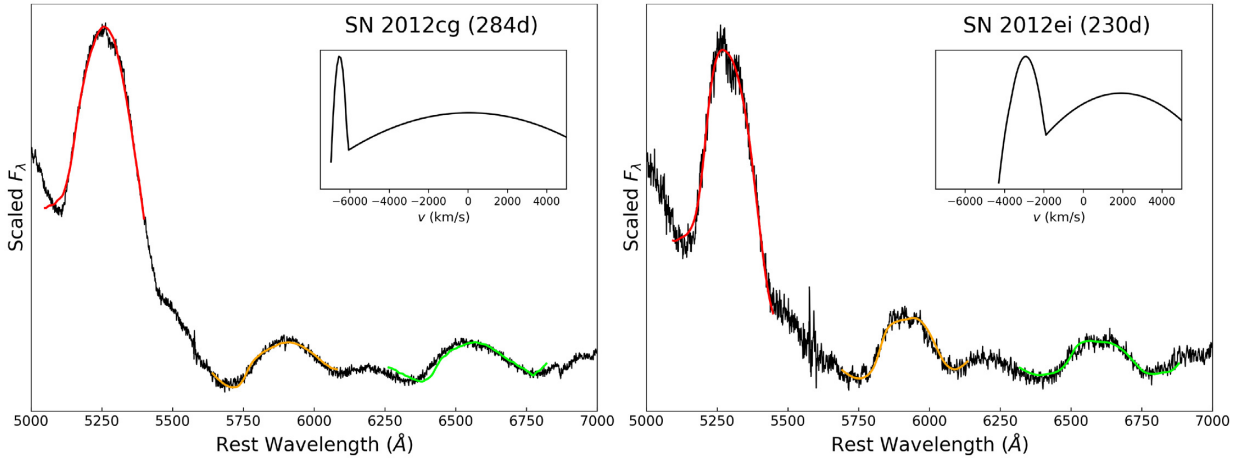

Figure 3. Two spectra representative of the single-component events we identify in our sample: SNe 2012cg and 2012ei. Fitting a convolution kernel to SN 2012cg is somewhat unnecessary, as the spectrum clearly does not show signatures of bimodality. SN 2012ei, however, does show some signs of bimodality with somewhat flat-topped emission features and a degree of double-peaked emission in the ∼5300 Å [Fe II] and [Fe III] feature. This demonstrates the importance of using an objective classification scheme. In both cases, we classify these spectra as single component because the best-fitting velocity kernel has components that are significantly overlapping. Both spectra were obtained using the LBT, and the SN 2012cg spectrum was previously published by Shappee et al. (2018).

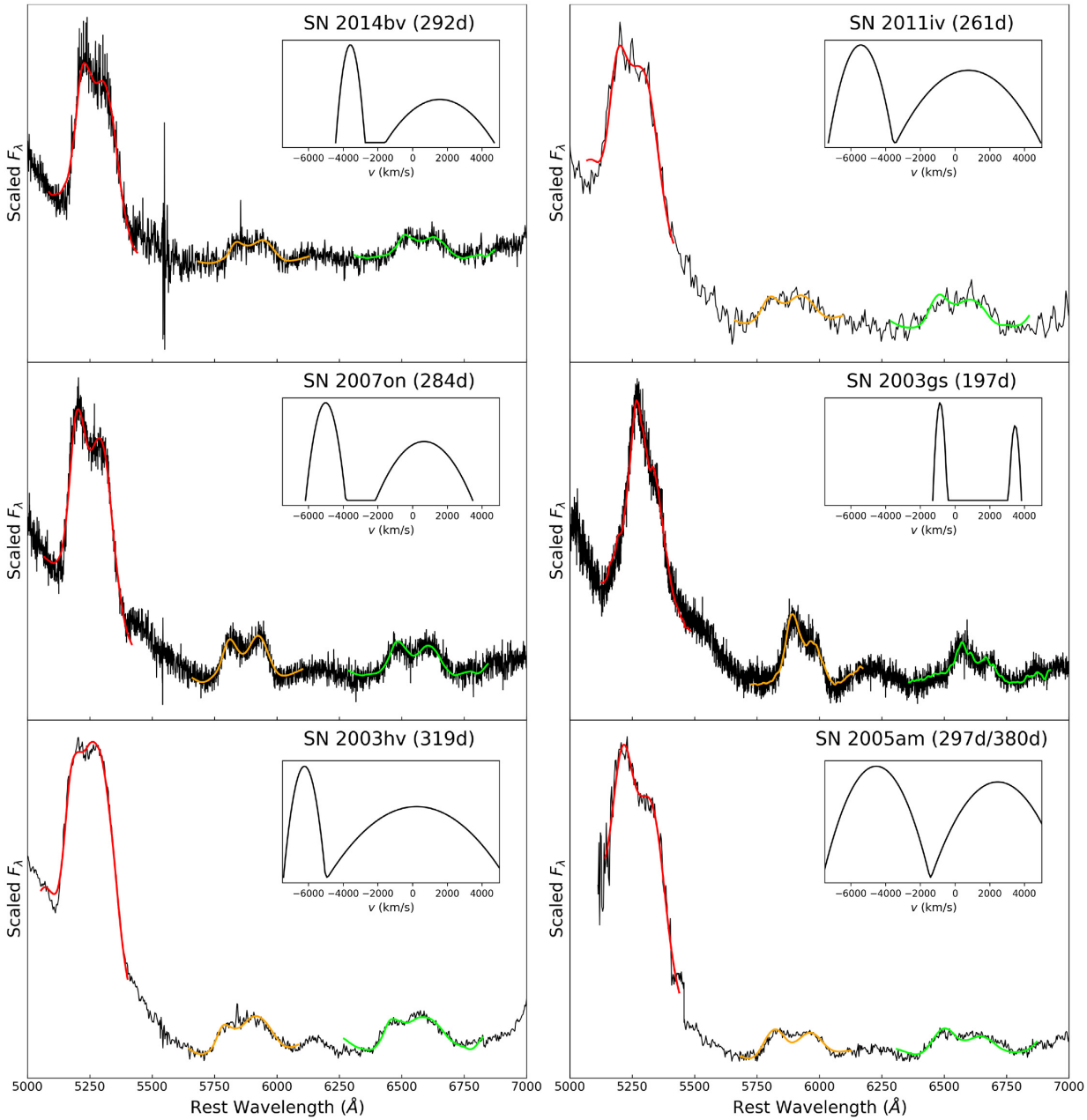

Figure 4. The six spectra we confidently identify as bimodal through multifeature fits to all three of the relevant ^{56}Ni decay features. In all cases, the two velocity kernel components are distinctly separated, and in most cases they are separated by a considerable margin. All of the fits appear reasonable upon inspection.

plicates interpretation of the [Co III] λ5891 emission feature. There is also some concern that a portion of the central minimum of the double-peaked ∼6600 Å [Co III]/[Fe II] feature may be an artefact introduced through oversubtraction of the host galaxy contribution.

While these complications may produce artificial absorption in the central regions of the emission features in question, they will not affect the wings (which are well matched by the best-fitting model, particularly so for the [Co III] λ5891 and ∼5300 Å [Fe II]/[Fe III] features). In fact the artificial absorption may help explain why the two features in question have dee per central minima than produced by the otherwise well-fitting convolution. Nevertheless, due to the difficulty of interpretation we regard this event as a tentative bimodal identification. It is denoted by the orange markers in subsequent figures.

4 DISCUSSION AND CONCLUSIONS

Fig. 6 shows the peak absolute V-band magnitude (M_V) distribution for all of the SNe Ia in our sample. This distribution is similar to the SNe Ia luminosity distribution found by Ashall et al. (2016a) when neglecting host galaxy extinction. Events shown in grey are consistent with an underlying single-component velocity profile, while those shown in red are identified as bimodal utilizing the classification scheme described in Section 3. The darker shade of

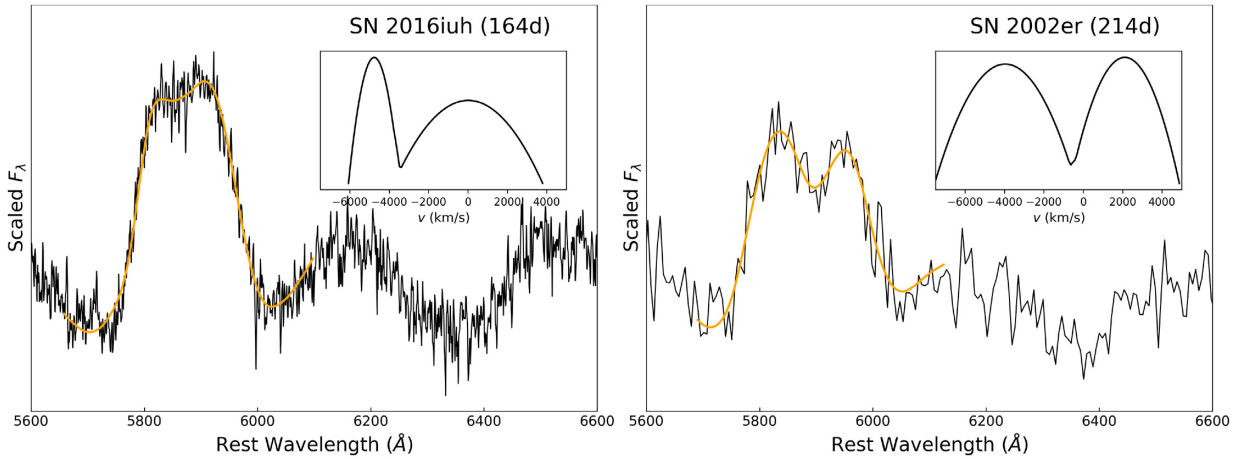

Figure 5. The two additional spectra we tentatively identify as bimodal based only on fits to the [Co III] λ5891 feature. While these identifications are less robust than those obtained using the multifeature fits, they appear to be consistent with the rest of the bimodal sample (see Section 4).

Table 4. Convolution fit parameters.

SN	$v_{\rm shift}$	$\sigma_{\rm mod,1}$	$\sigma_{\rm mod,2}$	$v_{\rm sep}$	r
SN 2014bv	−1007	847	3130	5154	0.441
SN 2011iv	−2327	1868	4163	6198	0.740
SN 2007on	−2170	1161	1799	5675	0.603
SN 2003gs	1300	425	373	4321	0.768
SN 2003hv	−2996	1211	5116	6460	0.636
SN 2005am	−1036	3083	3837	6999	0.858
SN 2016iuh	−2373	1307	3777	4776	0.658
SN 2002er	−926	3579	2770	6074	1.056
SN 1986G	−2255	1065	2178	4175	0.729
SN 2012cg	−3238	426	8368	6582	0.698
SN 2012ei	−592	1185	5581	5026	0.838

Notes. These fit parameters are the same as those described in Section 3. Note that velocities are presented in units of km s^{-1}.

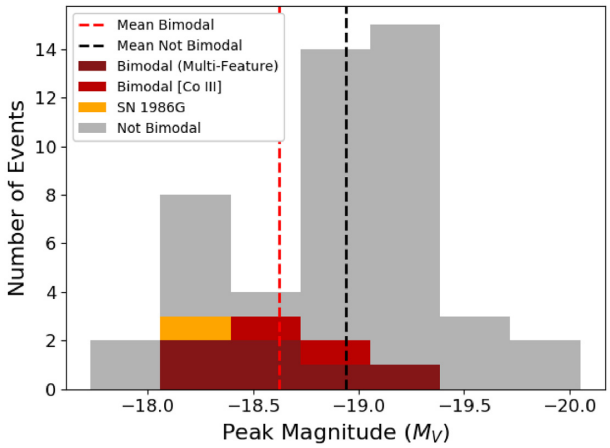

Figure 6. The distribution of peak M_V for our sample of SNe Ia. Spectra showing evidence of bimodal ^{56}Ni velocity profiles are shown in red, and those without such evidence are shown in grey. The different shades of red indicate whether a spectrum was identified as bimodal using fits to all three ^{56}Ni decay features (darker) or based only upon fits to the [Co III] λ5891 feature (lighter). Note that the average peak M_V for those events showing evidence of bimodal ^{56}Ni velocity profiles is fainter than those without such evidence by 0.32 mag.

red indicates an event confidently identified as bimodal using the multifeature fit criteria, while the lighter shade indicates an event whose [Co III] feature is consistent with bimodality.

The most striking characteristic of the bimodal events is their marked tendency towards fainter peak magnitudes. As noted by Dong et al. (2015) in their more limited sample, SNe Ia showing bimodal velocity profiles tend to have relatively large $\Delta m_{15}(B)$ values and be less luminous than those which do not. We find that the average peak M_V for events without signatures of bimodality is −18.94 mag (the vertical black dashed line in Fig. 6), while that of events with signatures of bimodality is −18.62 mag (the vertical red-dashed line in Fig. 6), a statistically significant offset of 0.32 mag. Using Welch's t-test we can conclude with 95.7 per cent confidence that the means of these two distributions are different ($t = 2.199$; $p = 0.043$), and using the two-sample Kolmogorov–Smirnov test we can conclude with 95.9 per cent confidence that the two distributions are distinct from one another ($D = 0.487$; $p = 0.041$).

Fig. 7 shows empirical comparisons of the bimodal sample relative to the rest of the SNe Ia population. The Phillips et al. (1999) decline rate versus peak luminosity relation we show in the figure is calibrated using the $M_{V,\rm peak}[\Delta m_{15}(B) = 1.1] = -19.12$ value from Folatelli et al. (2010), and we obtained the $\Delta m_{15}(B)$ values for our sample using SuperNovae in Object Oriented Python (Burns et al. 2011, 2014). We find that, when compared to the Phillips relation and a subsample of SNe Ia observed by the CSP, the bimodal SNe Ia are not significant outliers. Although they are systematically less luminous at maximum light, they still lie on the Phillips relation and do not show significantly more variance in absolute magnitude at fixed Δm_{15} than other SNe Ia.

We draw a similar conclusion when we examine the bimodal sample using the near-maximum spectroscopic subclasses identified by Branch et al. (2006), shown in the right-hand panel of Fig. 7 along with a large sample of SNe Ia from Blondin et al. (2012). The six bimodal SNe Ia for which there are publicly available near-maximum spectra appear consistent with the SNe Ia population at large. They do not fall into a limited range of the Branch diagram parameter space and are reasonably split among the four empirical classifications. These empirical characteristics of the bimodal sample are summarized in Table 5.

The tendency towards lower peak luminosities is consistent with observing collisional events at viewing angles of $\theta \sim 90°$, perpendicular to the collision axis ($\theta = 0°$). Using the Lagrangian

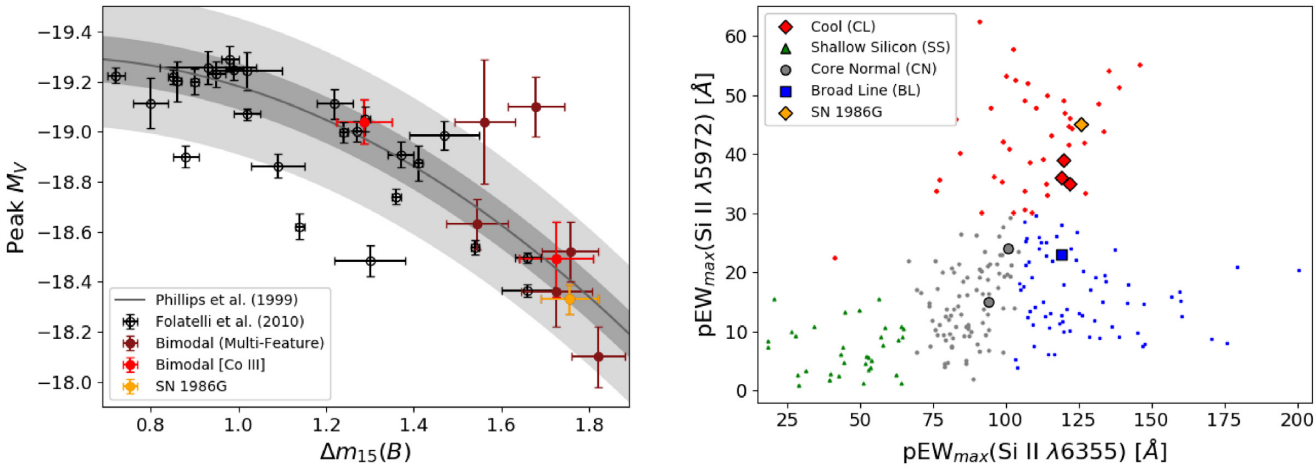

Figure 7. Empirical comparisons of the bimodal SNe Ia in our sample with the SNe Ia population at large. The left-hand panel shows the decline rate versus peak luminosity for bimodal events (shown in red) compared to the Phillips et al. (1999) relation. A sample of SNe Ia from Folatelli et al. (2010) is also included for comparison (shown in black). Events identified as bimodal using fits to all three ^{56}Ni decay features are shown using the darker red markers, while identifications based only upon fits to the [Co III] λ5891 feature are shown with the lighter red markers. The right-hand panel shows the pseudo-equivalent width (pEW) values for the Si II λ5972 and Si II λ6355 absorption features in near-maximum light spectra for six of the bimodal events (shown using the large symbols). The different symbols and colours correspond to the different subclasses defined by Branch et al. (2006). Formal pEW measurement uncertainties are of order 1 Å and are comparable in size to the symbols used to plot the bimodal events. We include the SNe Ia sample from Blondin et al. (2012) in this Branch diagram for comparison (shown using smaller symbols). Aside from their tendency towards lower peak luminosities, the bimodal SNe Ia do not appear to be significant outliers in either distribution.

Table 5. Empirical characteristics of the bimodal sample.

Name	Peak M_V	$\Delta m_{15}(B)$	Branch class
SN 2014bv	-18.36 ± 0.14	1.726 ± 0.080	–
SN 2011iv	-19.10 ± 0.12	1.679 ± 0.064	CL
SN 2007on	-18.52 ± 0.12	1.757 ± 0.064	CL
SN 2003gs	-18.10 ± 0.12	1.820 ± 0.061	–
SN 2003hv	-19.04 ± 0.25	1.562 ± 0.070	CN
SN 2005am	-18.63 ± 0.10	1.544 ± 0.070	BL
SN 2016iuh	-18.49 ± 0.15	1.725 ± 0.084	CL
SN 2002er	-19.04 ± 0.09	1.286 ± 0.063	BL
SN 1986G	-18.33 ± 0.06	1.756 ± 0.066	CL

Note. Branch classes are not reported for SNe 2014bv and 2003gs because there are no publicly available early phase spectra for these events.

hydrodynamics code of Rosswog et al. (2008) and Rosswog, Ramirez-Ruiz & Hix (2009a) and the 3D radiative transfer code SEDONA (Kasen, Thomas & Nugent 2006), Rosswog et al. (2009b) simulated explosions, and calculated synthetic light curves for WD–WD collisional detonations of varying WD masses. These simulated light curves are similar to those observed for SNe Ia. Rosswog et al. (2009b) also noted that, due to the asymmetry of the resultant ejecta, the observed properties of these SNe would exhibit some degree of viewing angle dependence. They found that the synthetic peak M_B could be reduced by as much as ∼0.5 mag when viewed edge on at $\theta \sim 90°$. This effect is similar in scale to that which we observe for this sample, although the synthetic light curves calculated by Rosswog et al. (2009b) have somewhat smaller $\Delta m_{15}(B)$ than the bimodal events in our sample.

Another potential physical explanation is that explosions produced through collisions of average mass WDs may synthesize less ^{56}Ni than other progenitor channels. Kushnir et al. (2013) calculated the ^{56}Ni yields (M_{56}) produced from collisional explosions for a range of binary WD masses. Their simulations showed that collisions between WDs of mass $0.55-0.65\,M_\odot$ produce between 0.2 and $0.4\,M_\odot$ of ^{56}Ni. This mass regime is important because the WD mass function is strongly peaked at $\sim 0.6\,M_\odot$ (Kepler et al. 2007). As shown by Piro, Thompson & Kochanek (2014), the combination of the WD mass function and the collisional model of Kushnir et al. (2013) predicts a ^{56}Ni yield distribution peaked near $0.3\,M_\odot$. Because the distribution of ^{56}Ni yields inferred from observed SNe Ia peaks at $M_{56} = 0.6\,M_\odot$ with an average value of $\sim 0.5\,M_\odot$ (Stritzinger et al. 2006; Wang et al. 2008), and because the peak Ia luminosity is directly connected with the synthesized ^{56}Ni mass, Piro et al. (2014) concluded that SNe Ia produced by collisions should be subluminous.

The expected scale of this effect can be estimated using the decline rate–nickel mass relation of Mazzali et al. (2007):

$$M_{56}/M_\odot = 1.34 - 0.67\Delta m_{15}(B), \quad (6)$$

and the V-band peak luminosity fit from Phillips (1993):

$$M_{V,\max} = -20.883 + 1.949\Delta m_{15}(B). \quad (7)$$

If the collisional WD channel produces SNe Ia with $M_{56} \sim 0.3\,M_\odot$, we would thus expect them to be ∼0.6 mag fainter than typical SNe Ia (with $M_{56} \sim 0.5\,M_\odot$), which is comparable to the effect observed in our sample.

We can estimate the critical viewing angle (θ_c, measured relative to the WD collision axis) beyond which we are no longer sensitive to identifying bimodal signatures. This critical angle is given by $\theta_c = 90° - \cos^{-1}(P_{\rm bimodal}/f)$, where $P_{\rm bimodal}$ is the proportion of observed SNe Ia for which we detect signatures of bimodality, and f is the fraction of all SNe Ia with intrinsic bimodal velocity components. Thus, if we assume that all SNe Ia have intrinsic bimodality, then we are sensitive to viewing angles up to $\theta_c \sim 10°$. If we assume instead that $f = 1/3$, then we are sensitive to viewing angles up to $\theta_c \sim 30°$. It seems unlikely that we would be sensitive to $\theta_c \gtrsim 45°$, so the fraction of SNe Ia with intrinsic bimodalility is probably not significantly smaller than 25 per cent.

A third potential explanation is that the method we use in this paper may simply be biased towards detecting bimodality in fainter SNe Ia. Abundance tomography studies indicate that ^{56}Ni is distributed out to considerably higher velocities in normal SNe Ia when compared to subluminous events. In the normal SN Ia 2011fe, ^{56}Ni is inferred to extend to velocities beyond 10 000 km s^{-1} (Mazzali et al. 2015), for example, while in the subluminous SN Ia 1986G it is inferred to extend only to about 6000 km s^{-1} (Ashall et al. 2016b). In order to observe signatures of bimodality, the two WDs need to collide with a velocity comparable to that of the ^{56}Ni region, so slower moving ^{56}Ni distributions would be more readily detectable.

However, this potential bias seems unlikely to be a significant effect. If this were a dominant effect one would expect to find numerous events with slightly overlapping velocity components that satisfy our single [Co III] feature fit criteria, and one would expect those events to be considerably brighter than the rest of the bimodal sample. We observe neither of those outcomes. It is important to note that abundance tomography studies generally assume a single-component model. When analyzing a spectrum that is comprised of two components, such an assumption would infer ^{56}Ni distributions extending to artificially high velocities. This can be seen clearly in the case of SN 2007on. When using a single-component model, ^{56}Ni in the ejecta is inferred to extend to velocities beyond 12 500 km s^{-1} (Ashall et al. 2018). The presence of ^{56}Ni at such high velocities would smear out any signature of bimodality, and yet we can clearly identify SN 2007on as a bimodal event (See Fig. 4). Detailed modeling by Mazzali et al. (2018) further confirms that the event is better reproduced using a model with two narrow velocity components instead of a single broad component.

It is now established that a non-negligible fraction of SNe Ia spectra exhibit features consistent with a bimodal ^{56}Ni velocity distribution. Dong et al. (2015) found that 3 of the 18 spectra they examined showed compelling evidence of bimodality. Here, we more than double the sample and find that 8 of 47 spectra show evidence of bimodality. The collisional WD scenario provides a possible explanation for these observed spectral properties, and the tendency towards fainter peak luminosities that we report here is also consistent with this theoretical picture. Further improvements will require larger statistical samples and more attention to possible selection effects as the statistical uncertainties on the bimodal fraction become smaller. Nevertheless, we can confidently assert that bimodal events are not rare, and any proposed combination of SNe Ia explosion scenarios must be able to produce a non-negligible fraction of them.

ACKNOWLEDGEMENTS

We thank the referee for helpful comments. All of the previously unpublished spectra presented in this paper were obtained with the MODS spectrographs built with funding from NSF grant AST-9987045 and the NSF Telescope System Instrumentation Program, with additional funds from the Ohio Board of Regents, and the Ohio State University Office of Research. The LBT is an international collaboration among institutions in the United States, Italy, and Germany. LBT Corporation partners are The Ohio State University, and The Research Corporation, on behalf of The University of Notre Dame, University of Minnesota, and University of Virginia; The University of Arizona on behalf of the Arizona university system; Istituto Nazionale di Astrofisica, Italy; LBT Beteiligungsgesellschaft, Germany, representing the Max-Planck Society, the Astrophysical Institute Potsdam, and Heidelberg University.

We thank Christa Gall for providing the data for SN 2011iv, and we are grateful to Todd Thompson for valuable comments. We thank the Las Cumbres Observatory (LCOGT) and its staff for its continuing support of the ASAS–SN project. We thank Subo Dong and Ping Chen for providing us with reduced photometry from LCOGT data for a number of events. ASAS–SN is supported by the Gordon and Betty Moore Foundation through grant GBMF5490 to the Ohio State University and NSF grant AST-1515927. Development of ASAS–SN has been supported by NSF grant AST-0908816, the Mt. Cuba Astronomical Foundation, the Center for Cosmology and AstroParticle Physics at the Ohio State University, the Chinese Academy of Sciences South America Center for Astronomy (CASSACA), the Villum Foundation, and George Skestos.

PJV is supported by the National Science Foundation Graduate Research Fellowship Program under grant DGE-1343012. MAT acknowledges support from the United States Department of Energy through the Computational Sciences Graduate Fellowship (DOE CSGF). KZS and CSK are supported by NSF grants AST-1515876, AST-1515927, and AST-1814440.

This research has used the NASA/IPAC Extragalactic Data base, which is operated by the Jet Propulsion Laboratory, California Institute of Technology, under contract with the National Aeronautics and Space Administration. This research has used NASA's Astrophysics Data System Bibliographic Services. IRAF is distributed by the National Optical Astronomy Observatory, which is operated by the Association of Universities for Research in Astronomy under a cooperative agreement with the National Science Foundation.

REFERENCES

Antognini J. M., Shappee B. J., Thompson T. A., Amaro-Seoane P., 2014, MNRAS, 439, 1079
Ashall C., Mazzali P., Sasdelli M., Prentice S. J., 2016a, MNRAS, 460, 3529
Ashall C., Mazzali P. A., Pian E., James P. A., 2016b, MNRAS, 463, 1891
Ashall C. et al., 2018, MNRAS, 477, 153
Barbon R., Ciatti F., Rosino L., 1982, A&A, 116, 35
Bildsten L., Shen K. J., Weinberg N. N., Nelemans G., 2007, ApJ, 662, L95
Blakeslee J. P., Lucey J. R., Barris B. J., Hudson M. J., Tonry J. L., 2001, MNRAS, 327, 1004
Blondin S. et al., 2012, AJ, 143, 126
Bloom J. S. et al., 2012, ApJ, 744, L17
Bottinelli L., Gouguenheim L., Paturel G., de Vaucouleurs G., 1985, A&AS, 59, 43
Branch D., Wheeler J. C., 2017, Supernova Explosions: Astronomy and Astrophysics Library. Springer-Verlag, Germany
Branch D., Lacy C. H., McCall M. L., Sutherland P. G., Uomoto A., Wheeler J. C., Wills B. J., 1983, ApJ, 270, 123
Branch D. et al., 2006, PASP, 118, 560
Brimacombe J. et al., 2018, Astron. Telegram, 11976, 1
Brown P. J. et al., 2012, ApJ, 753, 22
Brown P. J., Breeveld A. A., Holland S., Kuin P., Pritchard T., 2014, Ap&SS, 354, 89
Burns C. R. et al., 2011, AJ, 141, 19
Burns C. R. et al., 2014, ApJ, 789, 32
Cappellaro E. et al., 2001, ApJ, 549, L215
Cartier R. et al., 2017, MNRAS, 464, 4476
Childress M. J. et al., 2015, MNRAS, 454, 3816
Chomiuk L. et al., 2012, ApJ, 750, 164
Colgate S. A., McKee C., 1969, ApJ, 157, 623
Contreras C. et al., 2010, AJ, 139, 519
Contreras C. et al., 2018, ApJ, 859, 24
Dalcanton J. J. et al., 2009, ApJS, 183, 67

Dhawan S., Flörs A., Leibundgut B., Maguire K., Kerzendorf W., Taubenberger S., Van Kerkwijk M. H., Spyromilio J., 2018, A&A, 619, A102
di Serego-Alighieri S., Ponz J. D., 1987, in Danziger I. J., ed., European Southern Observatory Conference and Workshop Proceedings, Vol. 26, European Southern Observatory Conference and Workshop Proceedings. European Southern Observatory, Garching bei München, Germany, p. 545
Dong S., Katz B., Kushnir D., Prieto J. L., 2015, MNRAS, 454, L61
Dong S. et al., 2018, MNRAS, 479, L70
Fesen R. A., Höflich P. A., Hamilton A. J. S., Hammell M. C., Gerardy C. L., Khokhlov A. M., Wheeler J. C., 2007, ApJ, 658, 396
Folatelli G. et al., 2010, AJ, 139, 120
Folatelli G. et al., 2013, ApJ, 773, 53
Foley R. J. et al., 2014, MNRAS, 443, 2887
Galbany L. et al., 2016, MNRAS, 457, 525
Gall C. et al., 2018, A&A, 611, A58
Ganeshalingam M. et al., 2010, ApJS, 190, 418
García-Senz D., Cabezón R. M., Arcones A., Relaño A., Thielemann F. K., 2013, MNRAS, 436, 3413
Garnavich P. M. et al., 2004, ApJ, 613, 1120
Gerardy C. L. et al., 2007, ApJ, 661, 995
Gómez G., López R., 1998, AJ, 115, 1096
Goobar A. et al., 2014, ApJ, 784, L12
Graham M. L. et al., 2017, MNRAS, 472, 3437
Guillochon J., Parrent J., Kelley L. Z., Margutti R., 2017, ApJ, 835, 64
Hachisu I., Kato M., Nomoto K., 2012, ApJ, 756, L4
Hamers A. S., Pols O. R., Claeys J. S. W., Nelemans G., 2013, MNRAS, 430, 2262
Han Z., Podsiadlowski P., 2004, MNRAS, 350, 1301
Hawley W. P., Athanassiadou T., Timmes F. X., 2012, ApJ, 759, 39
Hicken M. et al., 2009, ApJ, 700, 331
Hicken M. et al., 2012, ApJS, 200, 12
Hill J. M., Green R. F., Slagle J. H., 2006, in Stepp L. M., ed., Proc. SPIE Conf. Ser. Vol. 6267, Ground-based and Airborne Telescopes. SPIE, Bellingham, p. 62670Y
Hillebrandt W., Kromer M., Röpke F. K., Ruiter A. J., 2013, Frontiers Phys., 8, 116
Höflich P., Khokhlov A. M., Wheeler J. C., 1995, ApJ, 444, 831
Höflich P., Gerardy C. L., Fesen R. A., Sakai S., 2002, ApJ, 568, 791
Höflich P., Gerardy C., Linder E., Marion H., 2003, in Alloin D., Gieren W., eds, Models for Type Ia Supernovae and Cosmology, Vol. 635. Springer-Verlag, Berlin, Heidelberg, p. 203
Holmbo S. et al., 2019, A&A, 627, A174
Hoyle F., Fowler W. A., 1960, ApJ, 132, 565
Iben I. Jr, Tutukov A. V., 1984, ApJS, 54, 335
Jha S. et al., 1999, ApJS, 125, 73
Kasen D., Thomas R. C., Nugent P., 2006, ApJ, 651, 366
Katz B., Dong S., 2012, preprint (arXiv:1211.4584)
Kepler S. O., Kleinman S. J., Nitta A., Koester D., Castanheira B. G., Giovannini O., Costa A. F. M., Althaus L., 2007, MNRAS, 375, 1315
Khokhlov A. M., 1991, A&A, 245, 114
Kochanek C. S. et al., 2017, PASP, 129, 104502
Kollmeier J. A. et al., 2019, MNRAS, 486, 3041
Kotak R. et al., 2005, A&A, 436, 1021
Kowalski M. et al., 2008, ApJ, 686, 749
Kozai Y., 1962, AJ, 67, 591
Krisciunas K. et al., 2009, AJ, 138, 1584
Kushnir D., Katz B., Dong S., Livne E., Fernández R., 2013, ApJ, 778, L37
Leloudas G. et al., 2009, A&A, 505, 265
Leonard D. C., 2007, ApJ, 670, 1275
Li W. et al., 2001, PASP, 113, 1178
Lidov M. L., 1962, Planet. Space Sci., 9, 719
Lira P. et al., 1998, AJ, 115, 234
Livio M., Riess A. G., 2003, ApJ, 594, L93
Livne E., 1999, ApJ, 527, L97
Lundqvist P. et al., 2013, MNRAS, 435, 329
Lundqvist P. et al., 2015, A&A, 577, A39
Maguire K. et al., 2012, MNRAS, 426, 2359
Maguire K., Taubenberger S., Sullivan M., Mazzali P. A., 2016, MNRAS, 457, 3254
Maoz D., Mannucci F., Nelemans G., 2014, ARA&A, 52, 107
Margutti R., Parrent J., Kamble A., Soderberg A. M., Foley R. J., Milisavljevic D., Drout M. R., Kirshner R., 2014, ApJ, 790, 52
Marion G. H. et al., 2015, ApJ, 798, 39
Mattila S., Lundqvist P., Sollerman J., Kozma C., Baron E., Fransson C., Leibundgut B., Nomoto K., 2005, A&A, 443, 649
Mazzali P. A., Röpke F. K., Benetti S., Hillebrandt W., 2007, Science, 315, 825
Mazzali P. A., Sauer D. N., Pastorello A., Benetti S., Hillebrandt W., 2008, MNRAS, 386, 1897
Mazzali P. A. et al., 2014, MNRAS, 439, 1959
Mazzali P. A. et al., 2015, MNRAS, 450, 2631
Mazzali P. A., Ashall C., Pian E., Stritzinger M. D., Gall C., Phillips M. M., Höflich P., Hsiao E., 2018, MNRAS, 476, 2905
McCully C. et al., 2014, ApJ, 786, 134
Moll R., Raskin C., Kasen D., Woosley S. E., 2014, ApJ, 785, 105
Motohara K. et al., 2006, ApJ, 652, L101
Munari U., Henden A., Belligoli R., Castellani F., Cherini G., Righetti G. L., Vagnozzi A., 2013, New Astron., 20, 30
Nomoto K., 1982, ApJ, 253, 798
Nomoto K., Iben I. Jr, 1985, ApJ, 297, 531
Pan Y.-C. et al., 2015, MNRAS, 452, 4307
Parodi B. R., Saha A., Sandage A., Tammann G. A., 2000, ApJ, 540, 634
Pastorello A. et al., 2007a, MNRAS, 377, 1531
Pastorello A. et al., 2007b, MNRAS, 376, 1301
Perlmutter S. et al., 1999, ApJ, 517, 565
Phillips M. M., 1993, ApJ, 413, L105
Phillips M. M. et al., 1987, PASP, 99, 592
Phillips M. M., Lira P., Suntzeff N. B., Schommer R. A., Hamuy M., Maza J., 1999, AJ, 118, 1766
Phillips M. M. et al., 2013, ApJ, 779, 38
Piersanti L., Gagliardi S., Iben, Icko J., Tornambé A., 2003, ApJ, 598, 1229
Pignata G. et al., 2004, MNRAS, 355, 178
Pignata G. et al., 2008, MNRAS, 388, 971
Piro A. L., Thompson T. A., Kochanek C. S., 2014, MNRAS, 438, 3456
Pogge R. W. et al., 2010, in McLean I. S., Ramsay S. K., Takami H., eds, Proc. SPIE Conf. Ser. Vol. 7735, Ground-based and Airborne Instrumentation for Astronomy III. SPIE, Bellingham, p. 77350A
Poznanski D., Prochaska J. X., Bloom J. S., 2012, MNRAS, 426, 1465
Prieto J. L. et al., 2019, preprint (arXiv:1909.05267)
Raskin C., Timmes F. X., Scannapieco E., Diehl S., Fryer C., 2009, MNRAS, 399, L156
Raskin C., Scannapieco E., Rockefeller G., Fryer C., Diehl S., Timmes F. X., 2010, ApJ, 724, 111
Richardson D., Thomas R. C., Casebeer D., Blankenship Z., Ratowt S., Baron E., Branch D., 2001, Bulletin of the American Astronomical Society, Vol. 33, American Astronomical Society Meeting Abstracts, 119th AAS Meeting. American Astronomical Society, Washington, D.C., p. 1428
Riess A. G. et al., 1998, AJ, 116, 1009
Riess A. G. et al., 2005, ApJ, 627, 579
Rosswog S., Ramirez-Ruiz E., Hix W. R., Dan M., 2008, Comput. Phys. Commun., 179, 184
Rosswog S., Ramirez-Ruiz E., Hix W. R., 2009a, ApJ, 695, 404
Rosswog S., Kasen D., Guillochon J., Ramirez-Ruiz E., 2009b, ApJ, 705, L128
Ruiz-Lapuente P., Lucy L. B., 1992, ApJ, 400, 127
Sand D. J. et al., 2018, ApJ, 863, 24
Sand D. J. et al., 2019, ApJ, 877, L4
Sasdelli M., Mazzali P. A., Pian E., Nomoto K., Hachinger S., Cappellaro E., Benetti S., 2014, MNRAS, 445, 711
Schlafly E. F., Finkbeiner D. P., 2011, ApJ, 737, 103
Shappee B. J., Stanek K. Z., Pogge R. W., Garnavich P. M., 2013, ApJ, 762, L5

Shappee B. J., Stanek K. Z., Kochanek C. S., Garnavich P. M., 2017, ApJ, 841, 48
Shappee B. J., Piro A. L., Stanek K. Z., Patel S. G., Margutti R. A., Lipunov V. M., Pogge R. W., 2018, ApJ, 855, 6
Shen K. J., Moore K., 2014, ApJ, 797, 46
Shen K. J., Bildsten L., Kasen D., Quataert E., 2012, ApJ, 748, 35
Silverman J., Foley R. J., Ganeshalingam M., Chornock R., Li W., Filippenko A. V., 2009, 213th AAS Meeting, Bulletin of the American Astronomical Society, Vol. 41, American Astronomical Society Meeting Abstracts #213. American Astronomical Society, Washington, D.C., p. 312
Silverman J. M. et al., 2012, MNRAS, 425, 1789
Silverman J. M., Ganeshalingam M., Filippenko A. V., 2013, MNRAS, 430, 1030
Sim S. A., Röpke F. K., Hillebrandt W., Kromer M., Pakmor R., Fink M., Ruiter A. J., Seitenzahl I. R., 2010, ApJ, 714, L52
Soker N., Kashi A., García-Berro E., Torres S., Camacho J., 2013, MNRAS, 431, 1541
Springob C. M., Masters K. L., Haynes M. P., Giovanelli R., Marinoni C., 2009, ApJS, 182, 474
Stanishev V. et al., 2007, A&A, 469, 645
Starrfield S., Truran J. W., Sparks W. M., Kutter G. S., 1972, ApJ, 176, 169
Stritzinger M., Mazzali P. A., Sollerman J., Benetti S., 2006, A&A, 460, 793
Takanashi N., Doi M., Yasuda N., 2008, MNRAS, 389, 1577
Thompson T. A., 2011, ApJ, 741, 82
Toonen S., Perets H. B., Hamers A. S., 2018, A&A, 610, A22
Tsvetkov D. Y., Metlov V. G., Shugarov S. Y., Tarasova T. N., Pavlyuk N. N., 2014, Contrib. Astron. Obs. Skalnate Pleso, 44, 67
Tucker M. A. et al., 2019, MNRAS, 00, 00
Tucker M. A., Shappee B. J., Wisniewski J. P., 2019, ApJ, 872, L22
Tully R. B., Rizzi L., Shaya E. J., Courtois H. M., Makarov D. I., Jacobs B. A., 2009, AJ, 138, 323
Tully R. B. et al., 2013, AJ, 146, 86
Tully R. B., Courtois H. M., Sorce J. G., 2016, AJ, 152, 50
Vallely P. et al., 2016, MNRAS, 460, 1614
Vallely P. J. et al., 2019, MNRAS, 487, 2372
Vinkó J. et al., 2012, A&A, 546, A12
Vinkó J. et al., 2018, PASP, 130, 064101
Wang B., Meng X.-C., Wang X.-F., Han Z.-W., 2008, Chin. J. Astron. Astrophys., 8, 71
Webbink R. F., 1984, ApJ, 277, 355
Wells L. A. et al., 1994, AJ, 108, 2233
Whelan J., Iben I. Jr, 1973, ApJ, 186, 1007
Woosley S. E., Weaver T. A., 1994, ApJ, 423, 371
Woosley S. E., Weaver T. A., Taam R. E., 1980, in Wheeler J. C., ed., Texas Workshop on Type I Supernovae. University of Texas, Austin, p. 96
Yang Y. et al., 2018, ApJ, 852, 89
Yaron O., Gal-Yam A., 2012, PASP, 124, 668
Yoon S. C., Langer N., 2005, A&A, 435, 967
Yoon S. C., Langer N., Scheithauer S., 2004, A&A, 425, 217
Zhai Q. et al., 2016, AJ, 151, 125

SUPPORTING INFORMATION

Supplementary data are available at *MNRAS* online.

Figure 1. The new LBT late-time SNe Ia spectra we present in this paper.

Please note: Oxford University Press is not responsible for the content or functionality of any supporting materials supplied by the authors. Any queries (other than missing material) should be directed to the corresponding author for the article.

This paper has been typeset from a TEX/LATEX file prepared by the author.